Nonlinear Analysis: Modelling and Control, Vol. 24, No. 6, 853–869
https://doi.org/10.15388/NA.2019.6.1

ISSN: 1392-5113
eISSN: 2335-8963

Influence of Soret and Dufour effects on unsteady 3D MHD slip flow of Carreau nanofluid over a slendering stretchable sheet with chemical reaction

Seethi Reddy Reddisekhar Reddy[a], **Polu Bala Anki Reddy**[a], **Ali J. Chamkha**[b,c]

[a]Department of Mathematics, SAS,
Vellore Institute of Technology,
Vellore-632014, India
pbarmaths@gmail.com

[b]Mechanical Engineering Department,
Prince Sultan Endowment for Energy and Environment,
Prince Mohammad Bin Fahd University,
Al-Khobar 31952, Saudi Arabia

[c]RAK Research and Innovation Center,
American University of Ras Al Khaimah,
P.O. Box 10021, Ras Al Khaimah, United Arab Emirates

Received: October 15, 2018 / **Revised:** January 4, 2019 / **Published online:** November 8, 2019

Abstract. This paper presents a numerical exploration on the unsteady three-dimensional hydromagnetic flow of Carreau nanofluid over a slendering stretchable sheet in the presence of thermal radiation and chemical reaction. Furthermore, the effects of velocity slip, thermal slip, solutal slip, Soret and Dufour are taken into account. The prevailing time-dependent partial differential equations are metamorphosed into a system of coupled nonlinear ordinary differential equations by using the appropriate similarity transformations. The resultant nonlinear coupled differential equations are solved numerically by using the Runge–Kutta fourth-order method along with shooting scheme. The sway of sundry parameters on velocity, temperature, concentration, shear stress, temperature gradient and concentration gradient has been premeditated, and numerical results are presented graphically and in tabular form. Comparison amid the previously published results, and the current numerical results are made for the limiting cases, which are found to be in a virtuous agreement.

Keywords: MHD, slendering stretchable sheet, thermal radiation, Soret and Dufour effects and chemical reaction.

1 Introduction

Nanofluids are solid-liquid materials, which contain nanometer-sized solid particles or else nanofibers with sizes 1–100 nm dispersed in a liquid such as oil, ethylene glycol, lubricants, water, biofluids and polymer solutions. During the recent decades, it has been

demonstrated that nanofluids exhibit improved thermos-physical properties such as altered viscosity, density, density thermal conductivity, thermal diffusivity and enhanced heat transfer rate when compared with traditional base fluids. Heat transfer of nanofluids are much interest in various areas of science, engineering and technology, chemical and nuclear industries and biomechanics. The term "nanofluid" was first formulated by Choi [5] to describe a new class of fluid. Later on, Buongiorno [4] employed a regenerated of convective transport in nanofluid flow by considering the effect of Brownian motion and thermophoresis. He noticed that Brownian motion and thermophoresis dominate the other important slip mechanisms in the nonappearance of turbulent effects. When small particles such as dust can be suspended in a gas with a temperature gradient, a power can be experienced in the direction of temperature gradient. The velocity of these particles, which efforts is from hot surface region to the cold surface region, is called thermophoretic velocity, and the force experienced by the deferred particle due to the temperature gradient is called thermophoretic force. The random movement of the suspended particles in a fluid is known as Brownian motion. So, it plays a vital role in many industrial applications such as in aerosol collection, nuclear reactor safety and removing small particles from gas streams. Sheikholeslami and Rashidi [32] investigated the variable magnetic field on nanofluid hydrothermal treatment considering Brownian motion and thermophoresis effects in a semi-annulus enclosure via CVFEM. The combined effects of variable viscosity, inclined Lorentz force on Williamson nanofluid flow over a variable stretching sheet was explored by Khan et al. [16]. Garoosi et al. [10] addressed the numerical simulation of the nanofluid in heat exchange square cavity using a Buongiorno model. The effect of nonuniform magnetic field in a lid driven semi-annulus enclosure filled with Fe_3O_4-water nanofluid was presented by Sheikholeslami et al. [33]. Das and Chatterjee [6] analyzed the thermophoresis and Brownian motion effect in heat transfer behaviour of a three-phase distribution transformer filled with nanofluid. The results of the parametric study show that nanofluid circulated with the magnetite nanoparticles has greater in maximum temperature (~ 11 K) followed by silica nanoparticles (~ 7.3 K) and quartz nanoparticles (~ 6 K). The combined effects of the thermophoresis and Brownian motion on convection heat transfer in an L-shape enclosure filled with a nanofluid using the control volume based finite element method was developed by Sheikholeslami et al. [31]. More recently, nanofluid models subject to various surfaces can be listed by several authors [3, 8, 9, 13, 14, 17, 18, 24, 30, 36].

The boundary layer flow over a stretching surface problem has been actively studied for decades because of its wide range applications such as aerodynamic extrusion of plastic sheets, the boundary layer along a liquid film in condensation processes, MHD generators, paper production, artificial fibers, drawing of copper wires, glass blowing, cooling of metallic sheets or electronic chips, metal spinning and many others. The combined effects of viscoelasticity and a magnetic field over a stretching surface was made by Andersson [2]. Rayapole and Jakkula [25] investigated the properties of Brownian motion and thermophoresis hydromagnetic flow on a stretching surface with inconsistent thickness. The effect of variable thickness on the steady 2D boundary layer flows of a nanoparticles TiO_2 and Ag with base fluid water through a slendering stretching sheet can be found by Acharya at al. [1]. Reddy et al. [29] investigated the effect of chemical

reaction as well as heat and mass transfer on the magneto-fluid dynamics flow of blood over an inclined permeable stretching surface with an acute angle α to the vertical in the presence of a nonuniform heat source/sink. The 3D flow of water-based SWNT and MWCNT nanofluids due to slendering nonlinear stretching sheet with slip effects were covered by Hayat et al. [11]. Many researchers [7,12,15,21,23,26–28,34,35] investigated the different flow problems over a stretching surface.

In all the above studies, Soret–Dufour effects were assumed to be negligible since the order of magnitude is lesser than the effect described by Fourier's and Fick's laws. It is significant when the species are introduced at a surface in the fluid domain with different (lower) density than the surrounding fluid. The phenomenon of thermo-diffusion in liquids was presented by Soret in 1879, and the difference of temperature caused by the gradient of species concentration was developed by Dufour in 1872. These effects play an important role in the field of geosciences, oceanography, chemical engineering and air pollution. Keeping in view its important applications, combined thermophoresis, Brownian motion and Dufour effects on natural convective heat transfer on nanofluids were investigated simultaneously by Pakravan and Yaghoubi [19]. Postelnicu [22] addressed the influence of a magnetic field over a vertical surface embedded in porous media considering diffusion-thermo and thermal-diffusion effects. Influence of thermophoresis and Soret and Dufour effects on hydromagnetic flow over a nonisothermal wedge with thermal radiation and ohmic dissipation was developed by Pal and Mondal [20].

To the best of authors' familiarity, no exploration has been made so far to examine the effects of Soret and Dufour on the hydromagnetic flow of slendering stretchable sheet in the presence of chemical reaction and thermal radiation. The current work ambitious to fill the gap in the existing literature. This type of studies finds their vigorous applications in heating development, cool organism, oceanography, artificial fibers etc. Inspired by the above-mentioned applications, the authors has focused on the problem, which addresses the numerical exploration on the unsteady three-dimensional MHD flow of Carreau nanofluid over a slendering stretchable sheet with thermal radiation and chemical reaction. Furthermore, the effects of velocity slip, thermal slip, solutal slip, Soret and Dufour are taken into account.

2 Governing equations and mathematical formulation

We consider the three-dimensional, incompressible MHD flow of an electrically conducting of Carreau nanofluid induced by a slendering stretchable sheet with multiple slip effects. We assume $z = J(1-mt)^{1/2}(x+y+c)^{(1-n)/2}$, where n represents the velocity power index parameter. Here $n = 1$ signifies the shape of surface yields to flat sheet, $n < 1$ and $n > 1$ are the shape of surface yields to outer convex and inner convex respectively, which are due to increment and reduction of wall thicknesses, and J is assumed small enough to keep the sheet adequately thin so that pressure gradient along the sheet may be ignored. Let x-axis be along the plane in an upward direction, y-axis is normal to it, and z-axis is normal to xy-plane. The coordinate system and flow model are shown in Fig. 1. At the time $t = 0$, the sheet is impulsively stretched with velocities

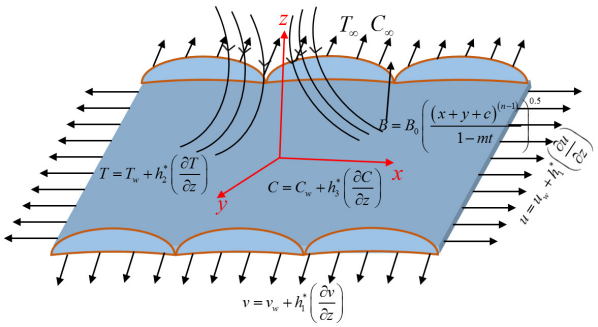

Figure 1. Physical configuration of the problem.

u_w, v_w along x- and y-axes, respectively. A magnetic field B is applied perpendicular to the sheet. To disregard the induced magnetic field, we take the magnetic Reynolds number as a very small quantity. Thermophoresis, Brownian motion, Soret–Dufour and time-dependent chemical reaction effects have been considered in this problem. Under these assumptions, the governing boundary layer along with the continuity, momentum, energy and concentration species can be written as (Das and Chatterjee [6], Pakravan and Yaghoubi [19] and Pal and Mondal [20])

$$\frac{\partial u}{\partial x}+\frac{\partial v}{\partial y}+\frac{\partial w}{\partial z}=0, \tag{1}$$

$$\begin{aligned}&\frac{\partial u}{\partial t}+u\frac{\partial u}{\partial x}+v\frac{\partial u}{\partial y}+w\frac{\partial u}{\partial z}\\&\quad=\nu\frac{\partial^2 u}{\partial z^2}\left(1+\Gamma^{*2}\left(\frac{\partial u}{\partial z}\right)^2\right)^{(n^*-1)/2}+\nu(n^*-1)\Gamma^{*2}\frac{\partial^2 u}{\partial z^2}\left(\frac{\partial u}{\partial z}\right)^2\\&\qquad\times\left(1+\Gamma^{*2}\left(\frac{\partial u}{\partial z}\right)^2\right)^{(n^*-3)/2}-\frac{\sigma B^2}{\rho_f}u,\end{aligned} \tag{2}$$

$$\begin{aligned}&\frac{\partial v}{\partial t}+u\frac{\partial v}{\partial x}+v\frac{\partial v}{\partial y}+w\frac{\partial v}{\partial z}\\&\quad=\nu\frac{\partial^2 v}{\partial z^2}\left(1+\Gamma^{*2}\left(\frac{\partial v}{\partial z}\right)^2\right)^{(n-1)/2}+\nu(n^*-1)\Gamma^{*2}\frac{\partial^2 v}{\partial z^2}\left(\frac{\partial v}{\partial z}\right)^2\\&\qquad\times\left(1+\Gamma^{*2}\left(\frac{\partial v}{\partial z}\right)^2\right)^{(n-3)/2}-\frac{\sigma B^2}{\rho_f}v,\end{aligned} \tag{3}$$

$$\begin{aligned}&\frac{\partial T}{\partial t}+u\frac{\partial T}{\partial x}+v\frac{\partial T}{\partial y}+w\frac{\partial T}{\partial z}\\&\quad=\alpha\frac{\partial^2 T}{\partial z^2}+\tau\left[D_B\frac{\partial C}{\partial z}\frac{\partial T}{\partial z}+\frac{D_T}{D_\infty}\left(\frac{\partial T}{\partial z}\right)^2\right]+\frac{16\sigma^* T_\infty^3}{3(\rho c)_f k^*}\frac{\partial^2 T}{\partial z^2}\\&\qquad+\frac{D_m k_T}{c_p c_s}\frac{\partial^2 C}{\partial z^2},\end{aligned} \tag{4}$$

$$\frac{\partial C}{\partial t} + u\frac{\partial C}{\partial x} + v\frac{\partial C}{\partial y} + w\frac{\partial C}{\partial z} = D_B\frac{\partial^2 C}{\partial z^2} + \frac{D_T}{T_\infty}\frac{\partial^2 T}{\partial z^2} - k_c(C - C_\infty) + \frac{D_m k_T}{T_m}\frac{\partial^2 T}{\partial z^2}. \tag{5}$$

The boundary conditions are

$$\begin{aligned} &u = u_w + h_1^*\frac{\partial u}{\partial z}, \qquad v = v_w + h_1^*\frac{\partial v}{\partial z},\\ &w = 0, \qquad T = T_w + h_2^*\frac{\partial T}{\partial z},\\ &C = C_w + h_3^*\frac{\partial C}{\partial z} \quad \text{at } z = J(1-mt)^{1/2}(x+y+c)^{(1-n)/2}\\ &u \to 0, \quad v \to 0, \quad T \to T_\infty, \quad C \to C_\infty \quad \text{as } z \to \infty, \end{aligned}$$

where

$$\begin{aligned} h_1^* &= \frac{2-f_1}{f_1}\xi_1\big((1-mt)(x+y+c)^{1-n}\big)^{1/2}, \qquad B = B_0\left(\frac{(x+y+c)^{n-1}}{1-mt}\right)^{1/2},\\ h_2^* &= \frac{2-b}{b}\xi_2\big((1-mt)(x+y+c)^{1-n}\big)^{1/2}, \qquad \xi_2 = \frac{2\gamma_1}{\gamma_1+1}\frac{\xi_1}{Pr},\\ h_3^* &= \frac{2-d}{d}\xi_3\big((1-mt)(x+y+c)^{1-n}\big)^{1/2}, \qquad \xi_3 = \frac{2\gamma_1}{\gamma_1+1}\frac{\xi_2}{Pr},\\ u_w &= U_0\frac{(x+y+c)^n}{1-mt}, \qquad v_w = U_0\frac{(x+y+c)^n}{1-mt},\\ T_w &= T_\infty + T_0\big((1-mt)(x+y+c)^{(1-n)}\big)^{1/2},\\ C_w &= C_\infty + C_0\big((1-mt)(x+y+c)^{(1-n)}\big)^{1/2}. \end{aligned}$$

In the above expressions, u, v and w are the components of velocities in x, y and z directions, respectively, Γ^* is the characteristic time constant, n^* is the power law index, ρ_f is the density of the nanofluid, σ is the electrical conductivity, σ^* is the Stefan–Boltzmann constant, k^* is the mean absorption coefficient, T is the temperature of the fluid, c_p is the specific heat at constant pressure, c_s is the concentration susceptibility, α is the thermal diffusivity, C is the concentration of the fluid, D_m is the coefficient of mean diffusivity, k_T is the thermal diffusion ratio, T_m is the mean fluid temperature, D_B is the Brownian diffusion coefficient, D_T is the thermophoresis diffusion coefficient, k_c is the chemical reaction rate, h_1^* is the dimensional velocity slip variable, h_2^* is the dimensional temperature jump variable, h_3^* is the dimensional concentration jump variable, f_1 is the Maxwell's reflection coefficient, b and d are the thermal and concentration accommodation coefficients, γ_1 is the ratio of specific heat, ξ_1, ξ_2, ξ_3 are the constants (mean free path), T_0, C_0 are the reference temperature and concentration of the fluid, T_∞, C_∞ are the temperature and concentration of the ambient fluid. The above partial differential

equations (1)–(5) and the corresponding boundary conditions can be rehabilitated into a system of coupled nonlinear ODE's by using the following similarity transformations (see Rayapole and Jakkula [25] and Acharya et al. [1]):

$$\begin{aligned}
&\zeta = \left(\frac{(n+1)U_0}{2\nu(1-mt)}\right)^{1/2}(x+y+c)^{(n-1)/2}z,\\
&\psi = \left(\frac{2\nu U_0}{(n+1)(1-mt)}\right)^{1/2}(x+y+c)^{(n+1)/2}F(\zeta),\\
&\Theta(\zeta) = \frac{T-T_\infty}{T_w-T_\infty}, \qquad \Phi(\zeta) = \frac{C-C_\infty}{C_w-C_\infty},\\
&u = U_0\frac{(x+y+c)^n}{1-mt}F'(\zeta), \qquad v = U_0\frac{(x+y+c)^n}{1-mt}G'(\zeta),\\
&w = -\left(\frac{2\nu U_0}{(n+1)(1-mt)}\right)^{1/2}(x+y+c)^{(n-1)/2}\\
&\quad\times\left[\frac{n+1}{2}\big(F(\zeta)+G(\zeta)\big)+\frac{n-1}{2}\zeta\big(F'(\zeta)+G'(\zeta)\big)\right],
\end{aligned} \tag{6}$$

where ζ is the similarity variable, and ψ is the stream function. Now substituting (6) into Eqs. (1)–(5), we get the following equations:

$$\begin{aligned}
&F'''\big(1+We^2F''^2\big)^{(n^*-3)/2}\big(1+n^*We^2F''^2\big)-A\frac{1}{n+1}(\zeta F''+2F')\\
&\quad-\frac{2n}{n+1}F'(F'+G')+F''(F+G)-M\frac{2}{n+1}F'=0,
\end{aligned} \tag{7}$$

$$\begin{aligned}
&G'''\big(1+We^2G''^2\big)^{(n^*-3)/2}\big(1+n^*We^2G''^2\big)-A\frac{1}{n+1}(\zeta G''+2G')\\
&\quad-\frac{2n}{n+1}G'(F'+G')+G''(F+G)-M\frac{2}{n+1}G'=0,
\end{aligned} \tag{8}$$

$$\begin{aligned}
&\frac{1}{Pr}\left(1+\frac{4}{3}R\right)\Theta''-A\frac{1}{n+1}(\zeta\Theta'+\Theta)+\frac{n-1}{n+1}\Theta(F'+G')\\
&\quad+\Theta'(F+G)+N_b\Theta'\Phi'+N_t\Theta'^2+Dr\Phi''=0,
\end{aligned} \tag{9}$$

$$\begin{aligned}
&\frac{1}{Sc}\Phi''-A\frac{1}{n+1}(\zeta\Phi'+\Phi)+\frac{n-1}{n+1}\Phi(F'+G')+\Phi'(F+G)\\
&\quad+\frac{1}{Sc}\frac{N_t}{N_b}\Theta''-\frac{2}{n+1}\Gamma\Phi+Sr\Theta''=0,
\end{aligned} \tag{10}$$

where $'$ denotes the differentiation with respect to ζ, A, We, M, Pr, R, N_b, N_t, Dr, Sr, Sc and Γ are the unsteadiness parameter, local Weissenberg number, magnetic parameter, Prandtl number, radiation parameter, Brownian motion, thermophoresis parameter, Dufour number, Soret number, Schmidt number and chemical reaction parameter,

respectively, which are given by

$$M=\frac{\sigma B_0^2}{\rho_f U_0},\qquad We=\frac{\Gamma^{*2}{U_0}^3(n+1)}{2\nu(1-mt)^3}(x+y+c)^{3n-1},$$
$$A=\frac{m}{U_0}(x+y+c)^{1-n},\qquad Pr=\frac{\mu c_p}{k},\qquad R=\frac{4\sigma^* T_\infty^3}{kk^*},$$
$$N_b=\frac{\tau D_B(C_w-C_\infty)}{\nu},\qquad N_t=\frac{\tau D_T(T_w-T_\infty)}{\nu T_\infty},\qquad Sc=\frac{\nu}{D_B},$$
$$Dr=\frac{D_B k_T(C_w-C_\infty)}{\nu c_p c_s(T_w-T_\infty)},\qquad Sr=\frac{D_B k_T(T_w-T_\infty)}{\nu T_m(C_w-C_\infty)}\qquad \gamma=\frac{k_0}{U_0}.$$

The corresponding boundary conditions are

$$\begin{aligned}
&F(\zeta)=\lambda\frac{1-n}{1+n}\big(1+\tau_1 F''(\zeta)\big),\quad F'(\zeta)=1+\tau_1 F''(\zeta),\quad \text{at } \zeta=\lambda,\\
&\Theta(\zeta)=1+\tau_2\Theta'(\zeta),\quad G(\zeta)=\lambda\frac{1-n}{1+n}\big(1+\tau_1 G''(\zeta)\big),\quad \text{at } \zeta=\lambda,\\
&G'(\zeta)=1+\tau_1 G''(\zeta),\quad \Phi(\zeta)=1+\tau_3\Phi'(\zeta)\quad \text{at } \zeta=\lambda,\\
&F'(\zeta)=0,\quad G'(\zeta)=0,\quad \Theta(\zeta)=0,\quad \Phi(\zeta)=0\quad \text{as } \zeta\to\infty.
\end{aligned}\tag{11}$$

Here λ is the wall thickness variable, τ_1 is the velocity slip variable, τ_2 is the temperature jump parameter, τ_3 is the concentration jump parameter:

$$\lambda=J\left(\frac{(n+1)U_0}{2\nu}\right)^{1/2},\qquad \tau_1=\frac{2-f_1}{f_1}\xi_1\left(\frac{(n+1)U_0}{2\nu}\right)^{1/2},$$
$$\tau_2=\frac{2-b}{b}\xi_2\left(\frac{(n+1)U_0}{2\nu}\right)^{1/2},\qquad \tau_3=\frac{2-d}{d}\xi_3\left(\frac{(n+1)U_0}{2\nu}\right)^{1/2}.$$

Equations (7)–(11) are nonlinear and coupled having the domain $[\lambda,\infty)$. In order to make the computations easier, it should be transformed as $[0,\infty)$. So, we establish a new function (see Khan et al. [16])

$$F(\zeta)=f(\zeta-\lambda)=f(\eta),\qquad G(\zeta)=g(\zeta-\lambda)=g(\eta),$$
$$\Theta(\zeta)=\theta(\zeta-\lambda)=\theta(\eta),\qquad \Phi(\zeta)=\phi(\zeta-\lambda)=\phi(\eta).$$

So, Eqs. (7)–(11) becomes

$$\begin{aligned}
&f'''\big(1+We^2 f''^2\big)^{(n^*-3)/2}\big(1+n^* We^2 f''^2\big)-A\frac{1}{n+1}\big((\eta+\lambda)f''+2f'\big)\\
&-\frac{2n}{n+1}f'(f'+g')+f''(f+g)-M\frac{2}{n+1}f'=0,
\end{aligned}\tag{12}$$

$$g'''\big(1+We^2g''^2\big)^{(n^*-3)/2}\big(1+n^*We^2g''^2\big)-A\frac{1}{n+1}\big((\eta+\lambda)g''+2g'\big)$$
$$-\frac{2n}{n+1}g'(f'+g')+g''(f+g)-M\frac{2}{n+1}g'=0, \tag{13}$$
$$\frac{1}{Pr}\left(1+\frac{4}{3}R\right)\theta''-A\frac{1}{n+1}\big((\eta+\lambda)\theta'+\theta\big)+\frac{n-1}{n+1}\theta(f'+g')$$
$$+\theta'(f+g)+N_b\theta'\phi'+N_t\theta'^2+Dr\phi''=0, \tag{14}$$
$$\frac{1}{Sc}\phi''-A\frac{1}{n+1}\big((\eta+\lambda)\phi'+\phi\big)+\frac{n-1}{n+1}\phi(f'+g')+\phi'(f+g)$$
$$+\frac{1}{Sc}\frac{N_t}{N_b}\theta''-\frac{2}{n+1}\Gamma\phi+Sr\theta''=0 \tag{15}$$

under the boundary conditions

$$\begin{aligned}
&f(0)=\lambda\frac{1-n}{1+n}\big(1+\tau_1f''(0)\big), \qquad f'(0)=1+\tau_1f''(0),\\
&g(0)=\lambda\frac{1-n}{1+n}\big(1+\tau_1g''(0)\big), \qquad g'(0)=1+\tau_1g''(0),\\
&\theta(0)=1+\tau_2\theta'(0), \qquad \phi(0)=1+\tau_3\phi'(0),\\
&f'(\infty)=0, \qquad g'(\infty)=0, \qquad \theta(\infty)=0, \qquad \phi(\infty)=0.
\end{aligned} \tag{16}$$

For the sake of engineering interest, skin friction coefficient, heat and mass transfer rates are

$$C_fRe_x^{1/2}=2\left(\frac{1+n}{2}\right)^{1/2}\big[1+We^2\big(f''(0)\big)^2\big]^{(n^*-1)/2}f''(0),$$
$$Nu_xRe_x^{-1/2}=-\left(\frac{1+n}{2}\right)^{1/2}\left(1+\frac{4}{3}R\right)\theta'(0),$$
$$Sh_xRe_x^{-1/2}=-\left(\frac{1+n}{2}\right)^{1/2}\phi'(0).$$

Here $'$ denotes the differentiation with respect to η (Eqs. (12)–(14)), $Re_x=u_w(x+y+c)/\nu_f$ is the local Reynolds number.

3 Discussion

The dimensionless governing flow equations (12)–(15) subject to the boundary conditions (16) are solved numerically by means of a proficient Runge–Kutta method of fourth-order using shooting scheme. The CPU took averagely 1.35 seconds to obtain the various profiles. We measured the values of nondimensional parameters as $We=0.5$, $n=0.6$, $\tau_1=0.2$, $\lambda=0.7$, $M=0.5$, $n^*=0.3$, $Pr=0.72$, $R=0.2$, $N_b=0.3$, $N_t=0.1$, $\tau_2=0.2$, $Dr=0.2$, $Sr=0.4$, $Sc=0.6$, $\tau_3=0.2$ and $\Gamma=0.5$. These

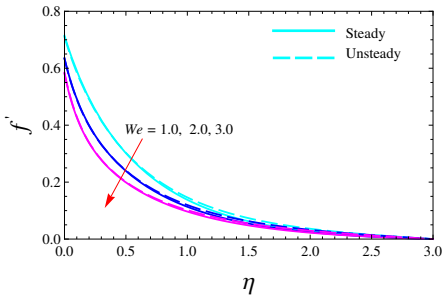

Figure 2. Effect of We on f'.

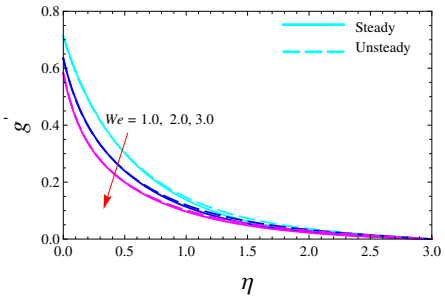

Figure 3. Effect of We on g'.

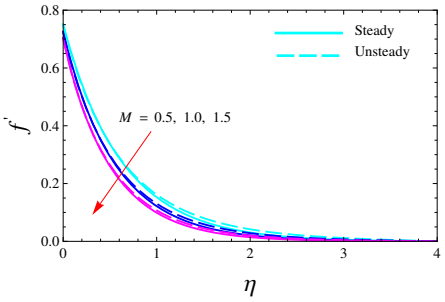

Figure 4. Effect of M on f'.

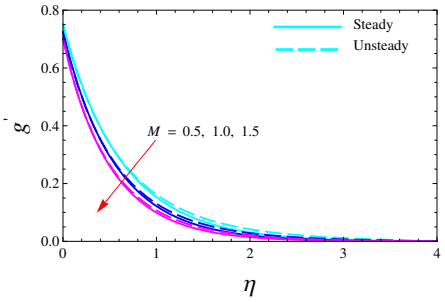

Figure 5. Effect of M on g'.

values have been not different all through the study apart from the values showed in figures. The effects of innumerable parameters are explored on the velocities, temperature and nanoparticle concentration profiles for both steady and unsteady cases, which are revealed in Figs. 2–24. Figures 2 and 3 represents the velocities profiles for the various values of local Weissenberg number (We). From these figures, it is perceived that the velocities of fluid decreases for hefty values of Weissenberg number in shear thinning fluid for both the cases of steady and unsteady. The impression of a magnetic parameter on the velocities profiles are demonstrated in Figs. 4 and 5. From these we detected that the velocities profile diminutions for both steady and unsteady cases with for soaring magnetic parameter. This is owed to the fact that an upsurge in magnetic parameter implies an enrichment of Lorentz force, thus falling the magnitude of the velocity. Figures 6 and 7 show the effect of velocities profiles for dissimilar values of wall thickness variable (λ). From these figures it is revealed that the velocities decrease with rising in wall thickness variable for the cases of steady and unsteady. The dimensionless velocities for numerous values of velocity slip variable (τ_1) are illustrated in Figs. 7 and 8. We observed that falls the velocities profile for both steady and unsteady cases with an increasing value of velocity slip variable. Figures 10 and 11 reveal the sway of velocities profiles for different values of power law index (n^*). It can be comprehended that the velocities enhance with an increase in power law index for both steady and unsteady cases. The outcome of temperature profiles for different values of Prandtl number (Pr) for both steady and unsteady cases is exhibited in Fig. 12. It is apparent that the thermal

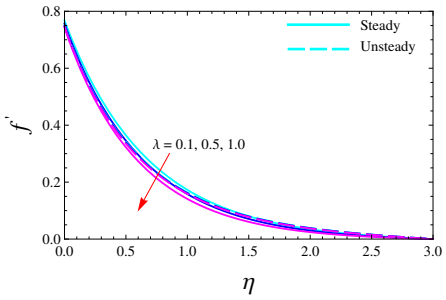

Figure 6. Effect of λ on f'.

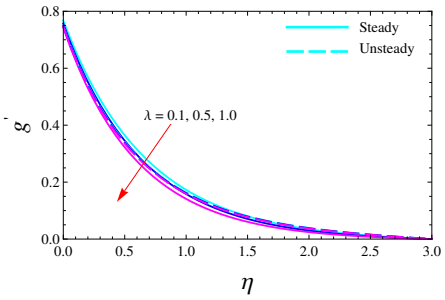

Figure 7. Effect of λ on g'.

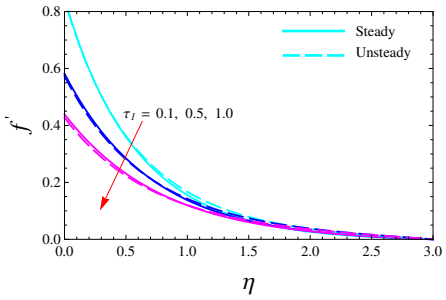

Figure 8. Effect of τ_1 on f'.

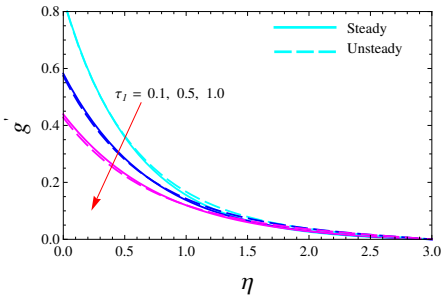

Figure 9. Effect of τ_1 on g'.

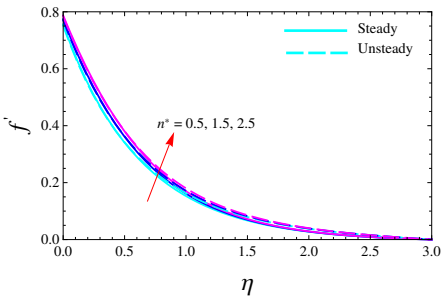

Figure 10. Effect of n^* on f'.

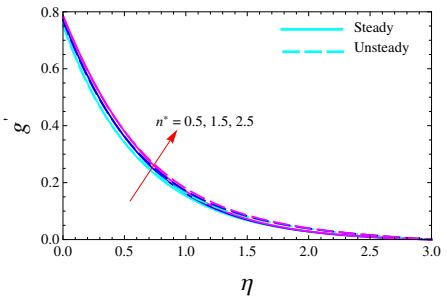

Figure 11. Effect of n^* on g'.

boundary layer is decreases due to an increase in Prandtl number for both steady and unsteady cases. Physically, thermal conductivity diminutions by increasing the Prandtl number lead to temperature profiles diminutions. Figure 13 illustrates the temperature profiles for different values of thermal radiation parameter (R). Here we witnessed from Fig. 13 that the temperature enriches (i.e., thermal boundary layer thickness increases) with increasing the values of thermal radiation parameter for both steady and unsteady cases. This is owed to fact that a rise in the values of $R = 4\sigma^* T_\infty^3/(kk^*)$ forgiven T_∞ and k means a diminution in the Rosseland radiation absorptivity k^*. According to the radiative heat flux with Rosseland approximation, the divergence of the radiative heat flux $\partial q_r/\partial y$ rises as k^* diminutions, which in turn leads to intensifications of the rate

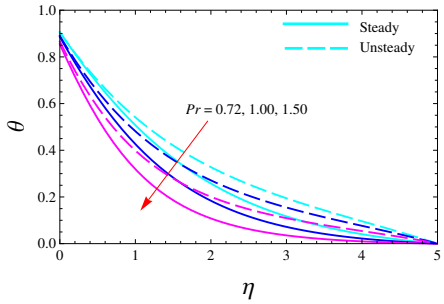

Figure 12. Effect of Pr on θ.

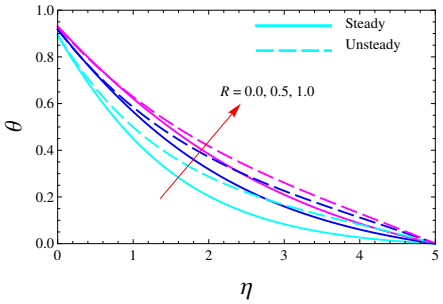

Figure 13. Effect of R on θ.

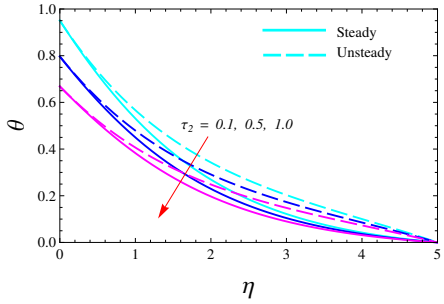

Figure 14. Effect of τ_2 on θ.

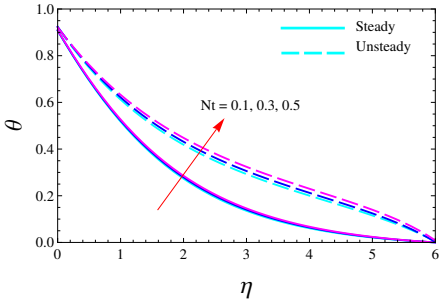

Figure 15. Effect of N_t on θ.

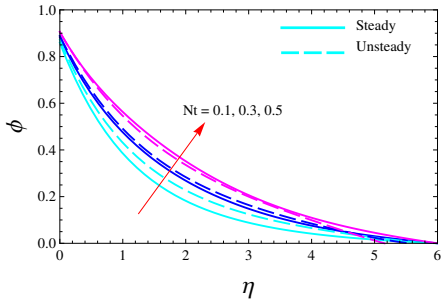

Figure 16. Effect of N_t on ϕ.

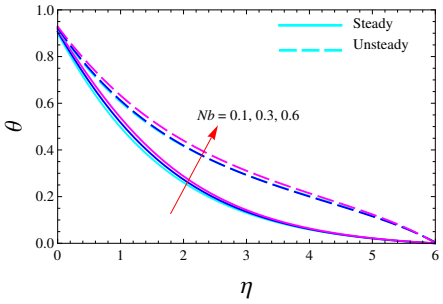

Figure 17. Effect of N_b on θ.

of radiative heat transferred to the fluid and hence the fluid temperature intensifications. The variations in the temperature profiles for changes in the temperature jump parameter (τ_2) are presented in Fig. 14. It can be inferred that an increase in the temperature jump parameter, decreases the temperature for both steady and unsteady cases. The impression of the thermophoresis parameter (N_t) on the temperature and concentration profiles is demonstrated in Figs. 15 and 16. From Fig. 15 we detected the temperature profiles intensifications for both steady and unsteady cases with for soaring thermophoresis parameter. Tangibly, thermophoresis is a mechanism in which small particles hauled away from the hot surface to the cold surface due to this reason temperature increases. From Fig. 16 we perceived the concentration profiles intensifications for both steady and unsteady

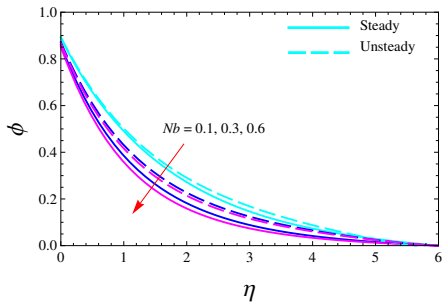

Figure 18. Effect of N_b on ϕ.

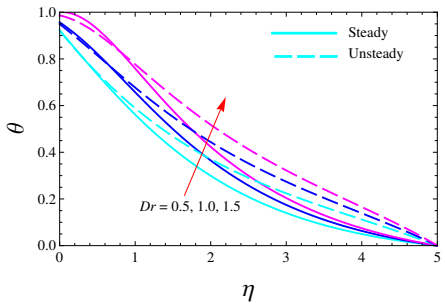

Figure 19. Effect of Dr on θ.

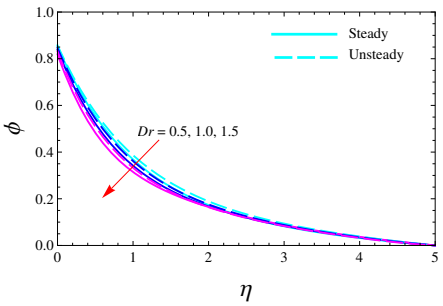

Figure 20. Effect of Dr on ϕ.

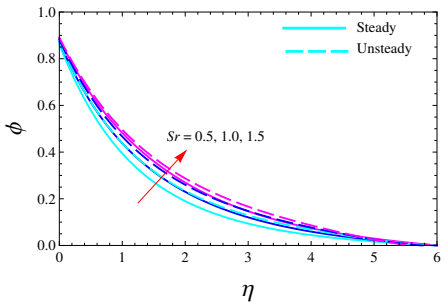

Figure 21. Effect of Sr on ϕ.

cases with the soaring thermophoresis parameter. Figures 17 and 18 show the effect of temperature and concentration profiles for dissimilar values of Brownian motion (N_b). From Fig. 17 it is revealed that the temperature profiles increase with the rise in Brownian motion for the cases of steady and unsteady. Figure 18 exposes the concentration profiles diminutions with rise in Brownian motion for the cases of steady and unsteady. This is due to the fact that, by increasing the values of Brownian motion parameter, the random motion of the microscopic particles increases, which diminishes the mass transfer rate. The dimensionless temperature and concentration distributions for numerous values of Dufour number (Dr) are illustrated in Figs. 19 and 20. We observed that temperature profiles increase and the concentration profiles decrease with rising in Dufour number for the cases of steady and unsteady. Figure 21 portrays the variation of concentration distribution for different values of Soret number (Sr). It can be perceived that the concentration distribution increases with increasing values of Soret number for both steady and unsteady cases. Figure 22 exemplifies the nanoparticle concentration profiles for different values of chemical reaction parameter (Γ). We beheld from Fig. 22 that the concentration diminishes with increasing the values of chemical reaction parameter (Γ) for both steady and unsteady cases. Concentration profile extremely diminishes with the generative chemical reaction $\Gamma < 0$ when compared to destructive chemical reaction $\Gamma > 0$ due to the fact that as $\Gamma < 0$, the last term in the momentum equation becomes positive and plays a crucial role. The variations in the concentration profiles for changes in the Schmidt number (Sc) are presented in Fig. 23. It can be inferred that the concentration profiles

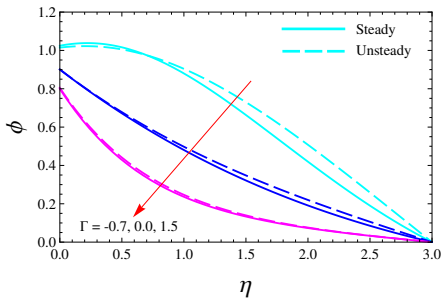

Figure 22. Effect of Γ on ϕ.

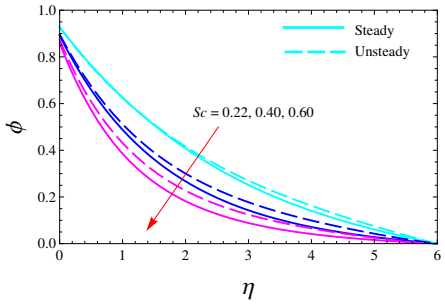

Figure 23. Effect of Sc on ϕ.

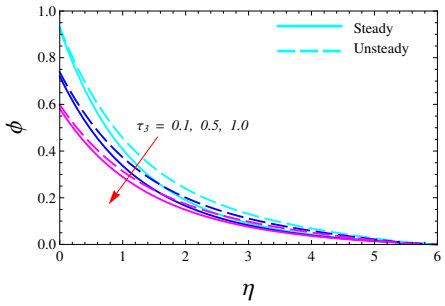

Figure 24. Effect of τ_3 on ϕ.

Table 1. Comparison of $-f''(0)$ for several values of velocity power index n with $A = 0$, $We = 0$, $M = 0$, $R = 0$, $N_b = 0$, $Sc = 0$, $\Gamma = 0$, $Sr = 0$, $Dr = 0$, $\lambda = 0$, $\tau_1 = 0$, $\tau_2 = 0$, $\tau_3 = 0$, $n^* = 0$.

n	10	5	3	2	1	0.5	0	−0.5
Fang et al. [7]	1.0603	1.0486	1.0359	1.0234	1	0.9799	0.9576	1.1667
Khader and Megahed [15]	1.0603	1.0486	1.0358	1.0234	1	0.9798	0.9577	1.1666
Present results	1.06034	1.04862	1.03588	1.02342	1	0.97994	0.95764	1.16666

decrease with an increase in the Schmidt number for both steady and unsteady cases. Tangibly, Schmidt number defined as the momentum to mass diffusivities ratio. Thus, for higher Schmidt number, the mass diffusivity diminutions, which is responsible for the reduction of concentration profiles. Figure 24 portrays the variation of concentration distribution for different values of velocity slip concentration jump parameter (τ_3). It can be perceived that the concentration distribution diminutions with increasing values of concentration jump parameter for both steady and unsteady cases.

In order to assess the precision of the present numerical results, we compared our numerical results with Fang et al. [28] and Khader and Megahed [25] for the limited case. This comparison is shown in Table 1. It can be perceived that the results are found to be in tremendous agreement with that of previous studies. Table 2 pageants the effects of the skin-friction coefficient for sundry values of pertinent parameters. It can be noted that the skin-friction coefficient increases with an increase in the wall thickness variable (λ), velocity slip variable (τ_1) and velocity power index (n), whereas the reverse trend is

Table 2. Values of $f''(0)$ and $C_f Re_x^{1/2}$ for various values of We, n, M, A, λ and τ_1 with $n^* = 0.3$, $Pr = 0.72$, $R = 0.2$, $N_b = 0.1$, $N_t = 0.1$, $\tau_2 = 0.3$, $Dr = 0.2$, $Sr = 0.4$, $Sc = 0.6$, $\tau_3 = 0.1$, and $\Gamma = 0.5$.

We	n	M	A	λ	τ_1	$F''(0)$	$C_f Re_x^{1/2}$
0.5	0.6	0.5	0.5	1.0	0.5	−0.850467	−1.65412
1	0.6	0.5	0.5	1.0	0.5	−0.89758	−3.56462
0.5	0.8	0.5	0.5	1.0	0.5	−0.829215	−1.7066
0.5	0.6	1	0.5	1.0	0.5	−0.912696	−1.7876
0.5	0.6	0.5	0.7	1.0	0.5	−0.852051	−1.65749
0.5	0.6	0.5	0.5	1.5	0.5	−0.848556	−1.65005
0.5	0.6	0.5	0.5	1.0	0.7	−0.707503	−1.35485

Table 3. Values of $-\theta'(0)$ and $Nu_x Re_x^{-1/2}$ for various values of Pr, A, R, N_b, N_t, Dr and τ_2 with $n^* = 0.3$, $We = 0.5$, $n = 0.6$, $\tau_1 = 0.5$, $\lambda = 1.0$, $M = 0.5$, $Sr = 0.4$, $Sc = 0.6$, $\tau_3 = 0.1$, and $\Gamma = 0.5$.

Pr	A	R	N_b	N_t	Dr	τ_2	$-\theta'(0)$	$Nu_x Re_x^{-1/2}$
0.72	0.5	0.2	0.1	0.1	0.2	0.3	0.421992	0.478092
1	0.5	0.2	0.1	0.1	0.2	0.3	0.49365	0.559276
0.72	0.7	0.2	0.1	0.1	0.2	0.3	0.428619	0.485601
0.72	0.5	0.4	0.1	0.1	0.2	0.3	0.387301	0.531166
0.72	0.5	0.2	0.3	0.1	0.2	0.3	0.395182	0.447718
0.72	0.5	0.2	0.1	0.2	0.2	0.3	0.432336	0.489812
0.72	0.5	0.2	0.1	0.1	0.4	0.3	0.381748	0.432498
0.72	0.5	0.2	0.1	0.1	0.2	0.5	0.385565	0.552549

Table 4. Values of $-\phi'(0)$ and $Sh_x Re_x^{-1/2}$ for various values of Sc, A, Γ, N_b, N_t, Sr and τ_3 with $n^* = 0.3$, $We = 0.5$, $n = 0.6$, $\tau_1 = 0.5$, $\lambda = 1.0$, $M = 0.5$, $Pr = 0.72$, $R = 0.2$, $\tau_2 = 0.3$, and $Dr = 0.2$.

Sc	A	Γ	N_b	N_t	Sr	τ_3	$-\phi'(0)$	$Sh_x Re_x^{-1/2}$
0.6	0.5	0.5	0.1	0.1	0.4	0.1	0.599481	0.536192
0.8	0.5	0.5	0.1	0.1	0.4	0.1	0.738383	0.66043
0.6	0.7	0.5	0.1	0.1	0.4	0.1	0.58426	0.522578
0.6	0.5	1	0.1	0.1	0.4	0.1	0.819842	0.733289
0.6	0.5	0.5	0.3	0.1	0.4	0.1	0.714181	0.638783
0.6	0.5	0.5	0.1	0.2	0.4	0.1	0.425803	0.38085
0.6	0.5	0.5	0.1	0.1	0.6	0.1	0.578884	0.51777
0.6	0.5	0.5	0.1	0.1	0.4	0.3	0.512378	0.458254

observed by increasing the values of local Weissenberg number (We), magnetic parameter (M) and the unsteadiness parameter (A). Further, from Table 3 one can note that the Nusselt number increases with an increase in the unsteadiness parameter (A), Prandtl number (Pr), and thermophoresis parameter (N_t), while it decreases with the increase of radiation parameter (R), Brownian motion (N_b), temperature jump parameter (τ_2) and Dufour number (Dr). Moreover, from Table 4 it can be found that the values of Sherwood number decreases as the unsteadiness parameter (A), thermophoresis parameter (N_t), Soret number (Sr) and concentration jump parameter (τ_3) increases, whereas the opposite effect is observed by increasing the values of the Schmidt number (Sc), chemical reaction parameter (Γ) and Brownian motion (N_b).

4 Main findings

A numerical solution has been presented for the unsteady, three-dimensional hydromagnetic flow of Carreau nanofluid over a slendering stretchable sheet with diffusion-thermo and thermal-diffusion effects. Thermal radiation, chemical reaction, thermophoresis, Brownian motion, velocity slip, thermal slip and concentration slips are considered. The governing nonlinear ordinary differential equations are solved numerically by using the Runge–Kutta fourth-order method along with shooting scheme. The main interpretations from this study can be abridged as follows:

1. Governing equations are nonlinear and coupled having the domain $[\lambda, \infty)$.
2. The velocities decrease with rising in the values of local Weissenberg number and wall thickness variable for the cases of steady and unsteady cases, whereas the opposite effect is observed by increasing in power law index for both steady and unsteady cases.
3. The temperature distribution increases with increasing values of Soret number for both steady and unsteady cases.
4. The concentration profile extremely diminishes with the generative chemical reaction $\Gamma < 0$ when compared to destructive chemical reaction $\Gamma > 0$.
5. The skin-friction coefficient increases with an increase in the wall thickness variable, velocity slip variable and velocity power index, whereas the reverse trend is observed by increasing the values of local Weissenberg number, magnetic parameter and the unsteadiness parameter.
6. The Nusselt number increases with an increase in the thermophoresis parameter, while it decreases with the increase of radiation parameter and Dufour number.
7. The Sherwood number decreases as the thermophoresis parameter, Soret number and concentration jump parameter increases, whereas the opposite effect is observed by increasing the values of the chemical reaction parameter and Brownian motion.

References

1. N. Acharya, K. Das, P. Kumar Kundu, Ramification of variable thickness on MHD TiO_2 and Ag nanofluid flow over a slendering stretching sheet using NDM, *Eur. Phys. J. Plus*, **131**(303):1–16, 2016.
2. H.I. Andersson, MHD flow of a viscoelastic fluid past a stretching surface, *Acta Mech.*, **95**(1–4):227–230, 1992.
3. M. Astanina, Dr.E. Abu-Nada, M.A. Sheremet, Combined effects of thermophoresis, Brownian motion and nanofluid variable properties on natural convection in a partially heated square cavity, *J. Heat Transfer*, **140**(8):082401, 2018.
4. J. Buongiorno, Convective transport in nanofluids, *J. Heat Transfer*, **128**(3):240–250, 2006.
5. S.U.S. Choi, J.A. Eastman, Enhancing thermal conductivity of fluids with nanoparticles, in *Proceedings of the ASME International Mechanical Engineering Congress and Exposition, November 12–17, 1995, San Francisco, CA*, ASME, 1995, pp. 99–105.

6. A.K. Das, S. Chatterjee, Analysis of thermophoresis and Brownian motion effect in heat transfer for nanofluid immersed distribution transformer, *Electrical Eng.*, **100**(3):1963–1974, 2018.
7. T. Fang, J. Zhang, Y. Zhong, Boundary layer flow over a stretching sheet with variable thickness, *Appl. Math. Comput.*, **218**(13):7241–7252, 2012.
8. N. Freidoonimehr, A.B. Rahimi, Brownian motion effect on heat transfer of a three-dimensional nanofluid flow over a stretched sheet with velocity slip, *J. Therm. Anal. Calorim.*, **135**(1): 207–222, 2019.
9. N. Freidoonimehr, M.M. Rashidi, S. Mahmud, Unsteady MHD free convective flow past a permeable stretching vertical surface in a nano-fluid, *Int. J. Therm. Sci.*, **87**:136–145, 2015.
10. Faroogh G., L. Jahanshaloo, M.M. Rashidi, A. Badakhsh, E. Mohammed Ali, Numerical simulation of natural convection of the nanofluid in heat exchangers using a Buongiorno model, *Appl. Math. Comput.*, **254**:183–203, 2015.
11. T. Hayat, Z. Hussain, A. Alsaedi, B. Ahmad, Numerical study for slip flow of carbon–water nanofluids, *Comput. Methods Appl. Mech. Eng.*, **319**:366–378, 2017.
12. E. Hosseini, G.B. Loghmani, M. Heydari, M.M. Rashidi, Numerical investigation of velocity slip and temperature jump effects on unsteady flow over a stretching permeable surface, *Eur. Phys. J. Plus*, **132**(96):1–16, 2017.
13. Z. Iqbal, R. Mehmood, Z. Mehmood, Thermal deposition on magnetohydrodynamic nanofluidic transport of viscoplastic fluid with microrotations, *J. Mol. Liq.*, **243**:341–347, 2017.
14. R. Kalaivanan, B. Ganga, N.V. Ganesh, A.K.A. Hakeem, Effect of elastic deformation on nano-second grade fluid flow over a stretching surface, *Front. Heat Mass Transfer*, **10**:20, 2018.
15. M.M. Khader, A.M. Megahed, Numerical solution for boundary layer flow due to a nonlinearly stretching sheet with variable thickness and slip velocity, *The Eur. Phys. J. Plus*, **128**(9):1–7, 2013.
16. M. Khan, M.Y. Malik, T. Salahuddin, A. Hussian, Heat and mass transfer of Williamson nanofluid flow yield by an inclined Lorentz force over a nonlinear stretching sheet, *Results Phys.*, **8**:862–868, 2018.
17. M. Khan, A. Shahid, M.Y. Malik, T. Salahuddin, Chemical reaction for Carreau–Yasuda nanofluid flow past a nonlinear stretching sheet considering Joule heating, *Results Phys.*, **8**:1124–1130, 2018.
18. Y. Lin, Y. Jiang, Effects of Brownian motion and thermophoresis on nanofluids in a rotating circular groove: A numerical simulation, *Int. J. Heat Mass Transfer*, **123**:569–582, 2018.
19. H.A. Pakravan, M. Yaghoubi, Combined thermophoresis, Brownian motion and Dufour effects on natural convection of nanofluids, *Int. J. Therm. Sci.*, **50**(3):394–402, 2011.
20. D. Pal, H. Mondal, Influence of thermophoresis and Soret–Dufour on magnetohydrodynamic heat and mass transfer over a non-isothermal wedge with thermal radiation and Ohmic dissipation, *J. Magn. Magn. Mater.*, **331**:250–255, 2013.
21. D. Pal, N. Roy, K. Vajravelu, Effects of thermal radiation and Ohmic dissipation on MHD Casson nanofluid flow over a vertical non-linear stretching surface using scaling group transformation, *Int. J. Mech. Sci.*, **114**:257–267, 2016.

22. A. Postelnicu, Influence of a magnetic field on heat and mass transfer by natural convection from vertical surfaces in porous media considering Soret and Dufour effects, *Int. J. Heat Mass Transfer*, **47**(6–7):1467–1472, 2004.

23. A.M. Rashad, Impact of thermal radiation on MHD slip flow of a ferrofluid over a non-isothermal wedge, *J. Magn. Magn. Mater.*, **422**:25–31, 2017.

24. A.M. Rashad, M.M. Rashidi, G. Lorenzini, S.E. Ahmed, A.M. Aly, Magnetic field and internal heat generation effects on the free convection in a rectangular cavity filled with a porous medium saturated with Cu–water nanofluid, *Int. J. Heat Mass Transfer*, **104**:878–889, 2017.

25. S.P. Rayapole, A.R. Jakkula, Effects of Brownian motion and thermophoresis on magneto hydrodynamics stagnation point of a nanofluid boundary layer flow on a stretching surface with variable thickness, *International Journal of Current Research and Review*, **9**(22):5–12, 2017.

26. P.B.A. Reddy, Magnetohydrodynamic flow of a Casson fluid over an exponentially inclined permeable stretching surface with thermal radiation and chemical reaction, *Ain Shams Eng. J.*, **7**(2):593–602, 2016.

27. P.B.A. Reddy, MHD boundary layer slip flow of a Casson fluid over an exponentially stretching surface in the presence of thermal radiation and chemical reaction, *Journal of Naval Architecture and Marine Engineering*, **13**:165–177, 2016.

28. P.B.A. Reddy, S. Suneetha, Effects of homogeneous-heterogeneous chemical reaction and slip velocity on MHD stagnation flow of a micropolar fluid over a permeable stretching/shrinking surface embedded in a porous medium, *Front. Heat Mass Transfer*, **8**(24):1–11, 2017.

29. S.R.R. Reddy, B.A.P. Reddy, S. Suneetha, Magnetohydrodynamic flow of blood in a permeable inclined stretching surface with viscous dissipation, non-uniform heat source/sink and chemical reaction, *Front. Heat Mass Transfer*, **10**:22, 2018.

30. K.U. Rehman, M.Y. Malik, M. Zahri, M. Tahir, Numerical analysis of MHD Casson Navier's slip nanofluid flow yield by rigid rotating disk, *Results Phys.*, **8**:744–751, 2018.

31. M. Sheikholeslami, A.J. Chamkha, P. Rana, R. Moradi, Combined thermophoresis and Brownian motion effects on nanofluid free convection heat transfer in an L-shaped enclosure, *Chin. J. Phys.*, **55**(6):2356–2370, 2017.

32. M. Sheikholeslami, M.M. Rashidi, Non-uniform magnetic field effect on nanofluid hydro-thermal treatment considering Brownian motion and thermophoresis effects, *J. Braz. Soc. Mech. Sci. Eng.*, **38**(4):1171–1184, 2016.

33. M. Sheikholeslami, M.M. Rashidi, D.D. Ganji, Effect of non-uniform magnetic field on forced convection heat transfer of Fe_3O_4–water nanofluid, *Comput. Methods Appl. Mech. Eng.*, **294**(1):299–312, 2015.

34. F.A. Soomro, R. ul Haq, Z.H. Khan, Q. Zhang, Passive control of nanoparticle due to convective heat transfer of Prandtl fluid model at the stretching surface, *Chin. J. Phys.*, **55**(4):1561–1568, 2017.

35. S. Srinivas, P.B.A. Reddy, B.S.R.V. Prasad, Effects of chemical reaction and thermal radiation on MHD flow over an inclined permeable stretching surface with non-uniform heat source/sink: An application to the dynamics of blood flow, *J. Mech. Med. Biol.*, **14**(5):1450067, 2014.

36. I. Ullah, S. Shafie, I. Khan, K.L. Hsiao, Brownian diffusion and thermophoresis mechanisms in Casson fluid over a moving wedge, *Results Phys.*, **9**:183–194, 2018.